HOKKAIDO UNIVERSITY

Title	Simulations of chlorofluorocarbons in and around the Sea of Okhotsk : Effects of tidal mixing and brine rejection on the ventilation
Author(s)	Uchimoto, K.; Nakamura, T.; Nishioka, J.; Mitsudera, H.; Yamamoto-Kawai, M.; Misumi, K.; Tsumune, D.
Citation	Journal of Geophysical Research, Oceans, 116, C02034 https://doi.org/10.1029/2010JC006487
Issue Date	2011-02-25
Doc URL	http://hdl.handle.net/2115/46975
Rights	Copyright 2011 by the American Geophysical Union.
Type	article
File Information	JGR116_C02034.pdf

Instructions for use

Hokkaido University Collection of Scholarly and Academic Papers : HUSCAP

Simulations of chlorofluorocarbons in and around the Sea of Okhotsk: Effects of tidal mixing and brine rejection on the ventilation

K. Uchimoto,[1] T. Nakamura,[1] J. Nishioka,[1] H. Mitsudera,[1] M. Yamamoto-Kawai,[2,3] K. Misumi,[4] and D. Tsumune[4]

Received 25 June 2010; revised 29 November 2010; accepted 21 December 2010; published 25 February 2011.

[1] Ventilation of waters in and around the Sea of Okhotsk was investigated using simulations of chlorofluorocarbons (CFCs) in the northwestern North Pacific. We used an ocean general circulation model coupled with a sea ice model. The model reproduces the distributions of CFCs similar to observed values and indicates the importance of tidal mixing along the Kuril Islands and brine rejection to ventilation of waters in and around the Sea of Okhotsk. To clarify the role of each process, numerical experiments excluding one of the two processes were carried out. Results show that brine rejection transports CFCs into the intermediate layer as deep as 200–400 m along the path of dense shelf water in the western Sea of Okhotsk, but hardly to other areas and layers. On the other hand, tidal mixing transports CFCs into the intermediate and deeper layers throughout the Sea of Okhotsk. We conclude that the tidal mixing has a greater influence than brine rejection on the ventilation of layers below the winter mixed layer.

Citation: Uchimoto, K., T. Nakamura, J. Nishioka, H. Mitsudera, M. Yamamoto-Kawai, K. Misumi, and D. Tsumune (2011), Simulations of chlorofluorocarbons in and around the Sea of Okhotsk: Effects of tidal mixing and brine rejection on the ventilation, *J. Geophys. Res.*, *116*, C02034, doi:10.1029/2010JC006487.

1. Introduction

[2] The Sea of Okhotsk is a marginal sea located in the northwestern corner of the Pacific (Figure 1). It is an important region for ventilation of the intermediate layer in the North Pacific [*Talley*, 1991], and thus has significant influences on the water properties, biogeochemical cycles and climate in the North Pacific [e.g., *Ono et al.*, 2003; *Nakanowatari et al.*, 2007; *Nishioka et al.*, 2007]. There are two processes contributing to the ventilation of the intermediate layer in the Sea of Okhotsk. One is the rejection of extremely salty water, called brine, during sea ice formation, and the other is diapycnal mixing around the Kuril Islands [e.g., *Talley*, 1991]. Sea ice is mainly produced on the northwestern shelf in the Sea of Okhotsk [e.g., *Martin et al.*, 1998; *Ohshima et al.*, 2003; *Nihashi et al.*, 2009] as a result of cold winds from the Siberian continent and freshwater discharge from the Amur River [*Ohshima et al.*, 2005]. As a result of brine rejection, cold, saline and well-ventilated water is formed on the shelf [*Kitani*, 1973; *Shcherbina et al.*, 2003]. This water is called dense shelf water (DSW). DSW flows out from the shelf southward along Sakhalin Island and eventually enters the intermediate layer in the deep areas of the Sea of Okhotsk [*Yamamoto et al.*, 2002; *Fukamachi et al.*, 2004]. A strong diapycnal mixing occurs along the Kuril Islands owing to strong tidal currents [*Nakamura and Awaji*, 2004; *Ono et al.*, 2007]. This tidal mixing is caused mainly through the generation and breaking of internal waves, and it thus reaches significant heights above the bottom boundary layer [*Nakamura et al.*, 2000]. Strong tidal mixing due to internal waves also occurs in the Atlantic Ocean [e.g., *Polzin et al.*, 1995] and in other oceans, though the dominant generation processes of internal waves are different: lee wave processes in the Kuril case and internal tide processes in the Atlantic case. This mixes the surface waters into deeper layers and ventilates these layers. Further, tidal mixing pumps salty water from the deeper layers up to the surface, and then the salty water is transported to the northwestern shelf. Tidal mixing along the Kuril Islands, therefore, contributes to the density and volume flux of DSW, because the density and volume flux depend on salinity in its production area [*Nakamura et al.*, 2006a; *Matsuda et al.*, 2009]. The well ventilated intermediate water formed by these processes in the Sea of Okhotsk flows out to the North Pacific and ventilates the intermediate layer in the North Pacific. In particular, the impact of the tidal mixing on the ventilation of the North Pacific Intermediate Water was discussed by *Nakamura et al.* [2006b].

[1] Pan-Okhotsk Research Center, Institute of Low Temperature Science, Hokkaido University, Sapporo, Japan.
[2] Department of Fisheries and Oceans, Institute of Ocean Sciences, Sidney, British Columbia, Canada.
[3] Now at Research Center for Advanced Science and Technology, Tokyo University of Marine Science and Technology, Tokyo, Japan.
[4] Environmental Science Research Laboratory, Central Research Institute of Electric Power Industry, Abiko, Japan.

Copyright 2011 by the American Geophysical Union.
0148-0227/11/2010JC006487

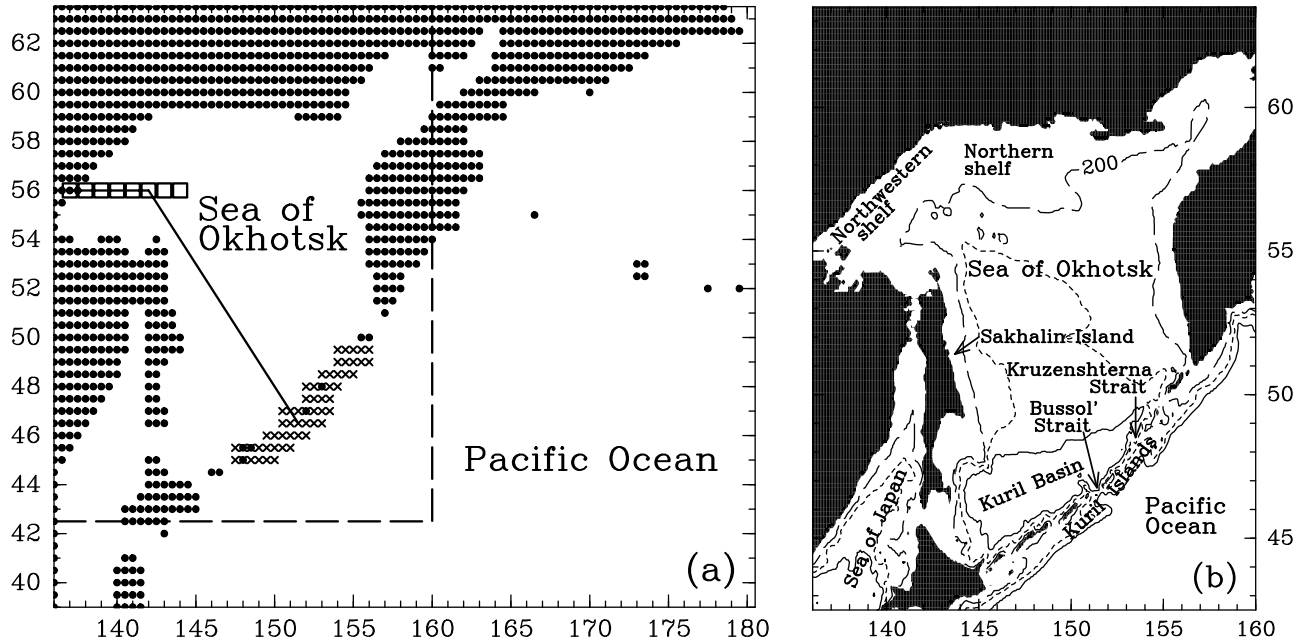

Figure 1. (a) Model domain. Model results are compared with observations along sections indicated as a solid line (Figure 7) and open squares (Figure 8). Large vertical diffusivity coefficients are given as tidal mixing effects at grid points denoted by crosses (along the Kuril Islands). The rectangular region with a broken line corresponds to Figure 1b. (b) Geography and bathymetry of the Sea of Okhotsk. Contours are drawn for 200 m (broken), 1000 m (dashed), and 2500 m (solid).

[3] Chlorofluorocarbons (CFCs) are among the most ideal chemical tracers to study ventilation processes. They are relatively recent (1930s) anthropogenic gasses and the history of atmospheric concentrations is known [*Walker et al.*, 2000]. They are inert gasses entering the ocean through air-sea gas exchange and are distributed in the ocean only by advection and diffusion. Consequently, distributions of CFCs in the ocean indicate the distribution of ventilated water. Thus, CFCs have been measured to study ventilation and circulation of the ocean (e.g., in the Pacific [*Watanabe et al.*, 1994, 1997; *Tokieda et al.*, 1996; *Warner et al.*, 1996; *Fine et al.*, 2001; *Mecking and Warner*, 2001] and in the Sea of Okhotsk [*Wong et al.*, 1998; *Yamamoto-Kawai et al.*, 2004, hereafter YK04]).

[4] In the Sea of Okhotsk, CFC concentrations are high in the intermediate layer around the 26.8 σ_θ density surface along the pathway of DSW from the northwestern shelf of the Sea of Okhotsk and along Sakhalin Island (YK04). This indicates that CFCs enter subsurface seawater on the northwestern shelf when DSW is formed, and are transported southward with DSW. In a deeper layer (27.4 σ_θ), the highest CFC concentrations were measured near Bussol' Strait. YK04 inferred that the deep layer was ventilated locally by tidal mixing. *Wong et al.* [1998] also mentioned that diapycnal mixing is necessary for CFCs to be transported into the deep layers.

[5] CFCs have also been used to evaluate ventilation processes in ocean models [e.g., *Dutay et al.*, 2002]. CFCs simulations for the North Pacific need improvement. In both global [e.g., *Dutay et al.*, 2002; *Ishida et al.*, 2007] and regional ocean models [e.g., *Sun et al.*, 2004], simulated CFCs do not penetrate as deep as observed in the North Pacific. Because the deepest ventilation in the North Pacific occurs in the Sea of Okhotsk, the failure in the North Pacific may be attributed to insufficient parameterization of ventilation processes in the Sea of Okhotsk in these models.

[6] In the present study, we simulated CFCs in the northwestern North Pacific using an ocean general circulation model (OGCM) including the effects of brine rejection and tidal mixing in the Sea of Okhotsk. The purpose of this study is to clarify the effects of tidal mixing along the Kuril Islands and brine rejection on ventilation of the intermediate and deeper layers. The OGCM is coupled with a sea ice model so that the sea ice formation/melting cycle is incorporated in the model. We apply a large diffusivity along the Kuril Islands to represent a strong tidal mixing in this region. As a result, the model has successfully reproduced CFCs distributions similar to those from cruise observations. In addition to the control simulation, we conducted two experiments each without one of the two processes, to evaluate the role of each process in the ventilation of the intermediate layer. Section 2 describes the model and hydrography in the model. Sections 3 and 4 show the results of the control simulation and the two experiments, respectively. A brief summary and concluding remarks are presented in section 5.

2. Model

2.1. Ocean and Sea Ice Model

[7] The OGCM used in the present study is the same as that used by *Matsuda et al.* [2009]: Center for Climate System Research Ocean Component Model version 3.4 coupled with a sea ice model (COCO [*Hasumi*, 2006]). COCO is a free surface model with the Boussinesq and hydrostatic approximation. We improved the model of *Matsuda et al.* [2009] to

cover a larger area and to have a better vertical resolution. The model domain spans the northwestern North Pacific, from 136°E to 179.5°W and from 39°N to 63.5°N (Figure 1a). The horizontal resolution is 0.5° in both zonal and meridional directions. There are 51 levels in the vertical direction with the thickness increasing from 1 m at the sea surface to 1000 m at the deepest level. The σ-coordinate system is applied for the top 11 levels, and the z-coordinate system is applied below them. The partial step formulation is adopted for the bottom topography [*Adcroft et al.*, 1997]. For the tracer advection, a uniformly third-order polynomial interpolation algorithm [*Leonard et al.*, 1994] is used, and isopycnal and thickness diffusion are used [*Cox*, 1987; *Gent et al.*, 1995]. The isopycnal and thickness diffusion coefficients are 1.0×10^6 and 3.0×10^6 cm^2/s, respectively, and background vertical viscosity and diffusion coefficients are 1.0 and 0.1 cm^2/s, respectively. The turbulence closure scheme of *Noh and Kim* [1999] is used.

[8] The sea ice model comprises thermodynamic and dynamic components. The thermodynamic part is the zero layer model by *Semtner* [1976]. The ice rheology in the dynamic part is an elastic-viscous-plastic formulation [*Hunke and Dukowicz*, 1997] with the eccentricity of the yield ellipse $e = 2$ and the ice strength parameter $P^* = 5.0 \times 10^3$ N/m^2. A two-category thickness representation is adopted, where the ice concentration and mean thickness are predicted in each grid. Sea ice is assumed to have salinity of 5 in the present study except one experiment (NObrine experiment in section 4).

[9] The model is forced at the sea surface by daily climatological atmospheric data concerning heat, freshwater, and momentum fluxes, which are taken from the Ocean Model Intercomparison Project (OMIP) data set [*Röske*, 2001]. Heat flux is calculated from the surface radiative fluxes, air temperature, humidity, and wind speed. Freshwater flux is formed from evaporation, sublimation, precipitation, and river runoff.

[10] Following *Matsuda et al.* [2009], we modified the freshwater data. In the northwestern shelf, the freshwater flux in the original OMIP data is high throughout the year with little seasonal variation. This is probably because the Amur River runoff is set to be almost constant throughout the year in the data. The Amur River runoff in winter is, however, only ~10% of runoff in summer because it freezes [*Ogi et al.*, 2001]. In order to add seasonality to the freshwater flux, we subtract the annual mean of the Amur River runoff from the freshwater data during the winter (from December to April) and evenly redistribute the subtracted amount in the other seasons to keep the total freshwater flux unchanged.

[11] Sea surface salinity (SSS) is restored to the monthly climatology of the World Ocean Atlas 2001 (WOA01 [*Conkright et al.*, 2002]) with 60 days of restoring time. The restoration is not applied in the northern half of the Sea of Okhotsk (≥ 52°N) in wintertime (from December to April), for the winter SSS of WOA01 in the Sea of Okhotsk is too low and is not reliable because of the lack of observations.

[12] Potential temperature (referred to as "temperature" hereafter) and salinity are restored to the WOA01 at a layer five grid points wide along the boundary. The surface elevation is restored to the output of a basin wide model at three grid points from the open boundaries. In addition, temperature and salinity are restored all over the Sea of Japan during the CFC experimental period. Also, at grid points deeper than about 2000 m, temperature and salinity are restored to the WOA01 with 10 days of restoring time in order to reduce the spin up time. This has insignificant effects on the equilibrium state, because the deep stratification is formed in the global thermohaline circulation.

[13] To incorporate tidal mixing effects into the model, a large vertical diffusivity coefficient is added to the value obtained by turbulent closure scheme around the Kuril Islands (crosses in Figure 1a) because the present model does not include tides.

[14] Although many numerical studies, for example, the main experiments by *Nakamura et al.* [2006a, 2006b] and *Matsuda et al.* [2009], used a vertically constant value of 200 cm^2/s, we applied a vertically varying coefficient; the value is set to be 500 cm^2/s at the bottom grid irrespective of the bottom depth, and decreases upward as shown by the thin solid line in Figure 2. The profile of vertical diffusivity coefficient in Figure 2 is based on the results that tidal mixing is stronger near the bottom in both a numerical experiment [*Nakamura and Awaji*, 2004] and an observational estimate (K. Ono, personal communication, 2010), and the use of this diffusivity profile improves the model hydrography.

[15] Reasonable values for the diffusivity are under discussion, because observations of vertical diffusivity along the Kuril Islands are limited. According to some Japanese reports [*Yagi and Yasuda*, 2008; *Itoh*, 2008], vertical diffusivities there are O(100) cm^2/s. In addition, *Nakamura et al.* [2010] reported that the maximum vertical diffusivity caused by tides exceeds 10^4 cm^2/s in the Aleutian passes. This intense mixing is caused through the breaking of internal lee waves, which also occurs in the Kuril Straits. The estimated values based on numerical simulations are O(10)-O(100) cm^2/s and exceed 1000 cm^2/s at limited regions such as over shallow sills [*Nakamura et al.*, 2000; *Nakamura and Awaji*, 2004]. In the estimate of *Tanaka et al.* [2007], although the averaged diffusivity around the Kuril Straits is 8 cm^2/s, values are O(100) cm^2/s along the Kuril Islands.

2.2. Method for CFC Experiments

[16] The CFC experiments were carried out from July 1931 to June 1997 after a 116 years spin-up. The ocean is initially at rest with constant temperature and salinity. During the first 2 years, temperature and salinity at all grid points are restored to the monthly climatology of WOA01. The CFC experiments were performed according to the protocols of the second phase of the Ocean Carbon Model Intercomparison Project (OCMIP-2), where the net CFC flux Q into the sea is given at the sea surface as

$$Q = k\left(FP_{\mathrm{CFC}}\frac{P}{P_0} - C_s\right), \tag{1}$$

where k is the air-sea gas transfer velocity, F is the CFC solubility function, which is a function of the sea surface temperature (SST) and SSS, P_{CFC} is the CFC atmospheric partial pressure, P is the air pressure at sea level, P_0 is 1 atm, and C_s is the concentration of CFCs at the sea surface. The method is specified in detail by *Dutay et al.* [2002]. In calculation of (1), we used temperature, salinity and the concentration of CFCs at the first level in the model as SST,

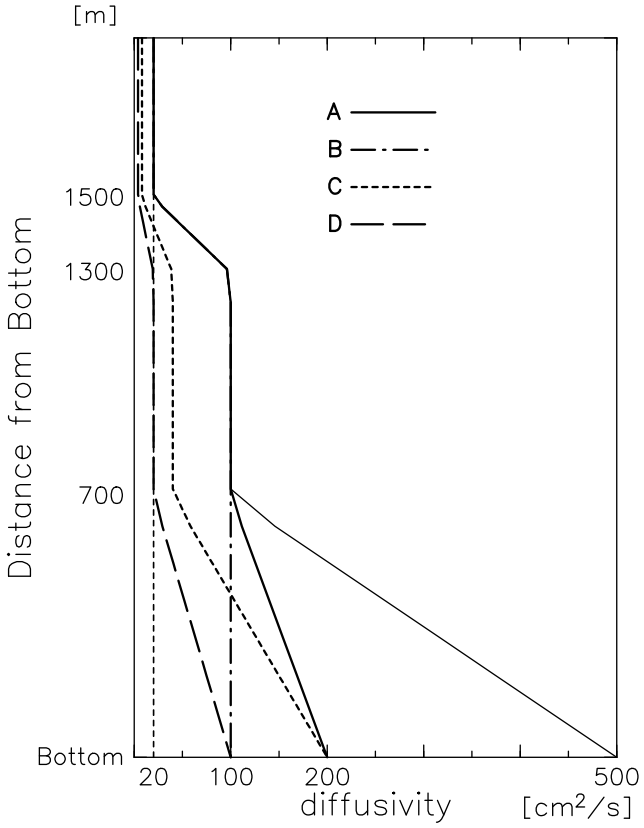

Figure 2. Vertical profiles of vertical diffusivity coefficient as a function of distance from the bottom, used in the model to represent the tidal mixing along the Kuril Islands (thin solid line). For the other lines (lines A, B, C, and D), see Appendix A.

SSS and C_s. For the other variables, we used the data provided by OCMIP-2. Generally speaking, when sea ice covers the sea, air-sea gas exchange hardly occurs there. This effect is included in air-sea gas transfer velocity, k, in the formulation of (1). We use the sea ice fraction data provided by OCMIP-2, not the outputs from the model itself, because the global mean of k is calibrated using those data [*Dutay et al.*, 2002]. Hence, the calculation of (1) does not depend on whether the sea surface in the model is covered with sea ice or not. As there is little ice in the Sea of Okhotsk in the OCMIP-2 ice data, we shall discuss effects of the ice concentration on the distributions of CFCs in section 5. CFCs are restored to 0 at the five grid points from the side open boundaries, and the CFCs fluxes at the sea surface are not given there, to prevent an artificial recirculation of CFCs in the model domain. Note that the physical part of the model is driven by atmospheric daily climatological data (see section 2.1) throughout the simulation period. Although we simulated both CFC-11 and CFC-12, we shall show only the results of CFC-12 below because almost the same results were found for CFC-11 except for the quantitative difference in the values of the concentration.

2.3. Circulations and Hydrography in the Model

[17] The model reproduces the physical oceanographic properties in the Sea of Okhotsk reasonably well, considering its 0.5° resolution. Ice distribution in the model (Figure 3a) is similar to an observational climatology estimation by *Ohshima et al.* [2006] (Figure 3b), but the concentration in the model is somewhat higher than in the climatological observation.

[18] Although the ice concentration is higher than 95% over the northern and the northwestern shelf areas in the model, we find somewhat low ice concentration (<95%) areas along the northern and the northwestern coastal areas in the model even in midwinter. This shows that coastal polynyas, where the formation of sea ice and the associated rejection of brine actively occur [*Kimura and Wakatsuchi*, 2004; *Nihashi et al.*, 2009], are represented in the model.

[19] The cyclonic gyre that features in the Sea of Okhotsk forms as shown in the barotropic stream function in March (Figure 4a). The strength of the gyre weakens in summer (not shown), indicating that seasonal variation is also represented in the model. The model also captures the following properties of the intermediate layer found in observations [*Itoh et al.*, 2003]. Low-temperature water on the 26.8 σ_θ

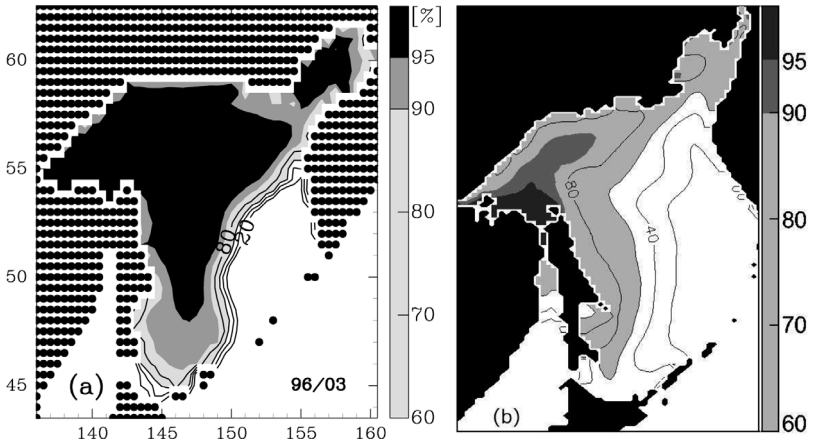

Figure 3. Ice concentration in March. (a) Model results and (b) observational climatology that is the monthly mean during 1978–2001 derived from SMMR and SSM/I [*Ohshima et al.*, 2006] (courtesy of S. Nihashi and K. I. Ohshima).

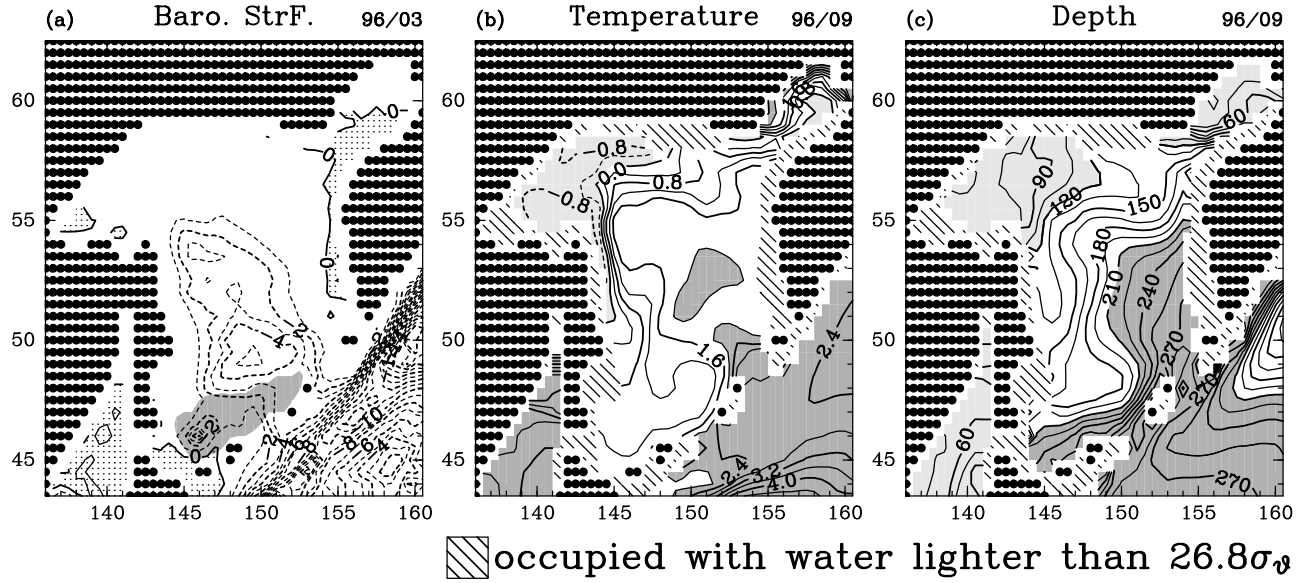

Figure 4. (a) Barotropic stream function (Sv = 10^6 m^3/s) in March. Dotted areas denote positive values. The shaded region denotes the Kuril Basin (bottom depths greater than 2500 m). (b) Potential temperature and (c) depth on the 26.8 σ_θ surface in September. Dense (light) shade in Figures 4b and 4c indicates areas with temperature higher than 2°C (lower than 0°C) and areas with depths deeper than 210 m (shallower than 120 m), respectively.

density surface extends from the northwestern shelf southward along Sakhalin Island, and high-temperature water extends from Kruzenshterna Strait to the north (Figure 4b). The depth of the 26.8 σ_θ surface is deep around the Kuril Islands and along the Kamchatka peninsula, while it is relatively shallow in the northern area and along Sakhalin Island (Figure 4c).

[20] Compared to the simulation by *Matsuda et al.* [2009], the present model better reproduces temperature along the Kuril Islands and the seasonal variation of the cyclonic gyre. Vertical profiles of temperature, salinity, and density in Bussol' Strait in the present study resemble those of observations by *Ono et al.* [2007] (Figure 5) better than those in the simulation by *Matsuda et al.* [2009]. This improvement of temperature along the Kuril Islands is due to a better parameterization of tidal mixing. The seasonal variation of the cyclonic gyre in the simulation by *Matsuda et al.* [2009] was much weaker than the present result and observations. In our model, we made Kruzenshterna Strait deeper and wider than in the model of *Matsuda et al.* [2009] to help water exchange between the Pacific and the Sea of Okhotsk. This may result in intensifying the seasonal variation of the circulation in the Sea of Okhotsk.

3. Standard Experiment

[21] We compare the simulated CFC-12 distribution with the data by YK04 and the data from the NODC Cruise SU-14129 in the World Ocean Database [*Johnson et al.*, 2009], which we refer to as "WOD data" hereafter. The WOD data include data observed in September 1993 on the World Ocean Circulation Experiment line P1W (the line from Bussol' Strait to the northwestern corner of the Sea of Okhotsk) [*Wong et al.*, 1998] and data at two points near the northern edge of the Kuril Basin (Figure 6a). These observational data give us a picture of the distribution of CFCs in the Sea of Okhotsk, their observations are spatially limited in the western part. Numerical simulations can compensate for the observational limitation and enable us to extend

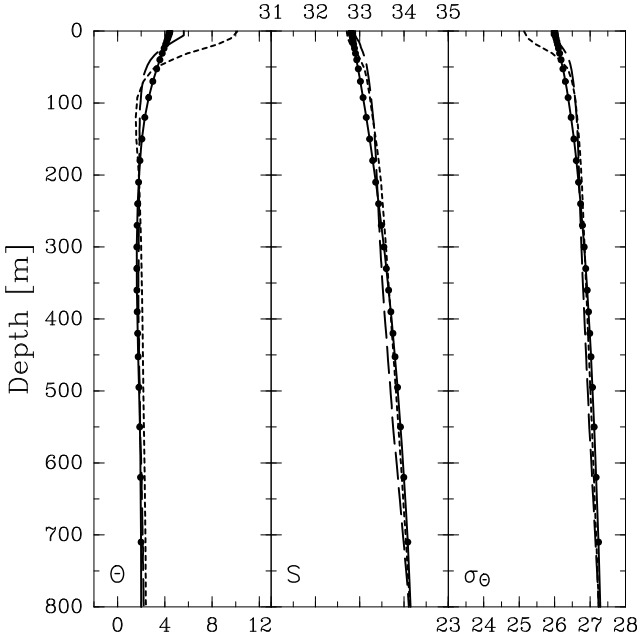

Figure 5. Vertical profiles of temperature (θ), salinity (S), and potential density (σ_θ). Model results (solid lines with dots), observation by *Ono et al.* [2007] (broken lines), and WOA01 (dashed lines) are shown. Model results and WOA01 are data of September, and the observation by *Ono et al.* [2007] was carried out in September.

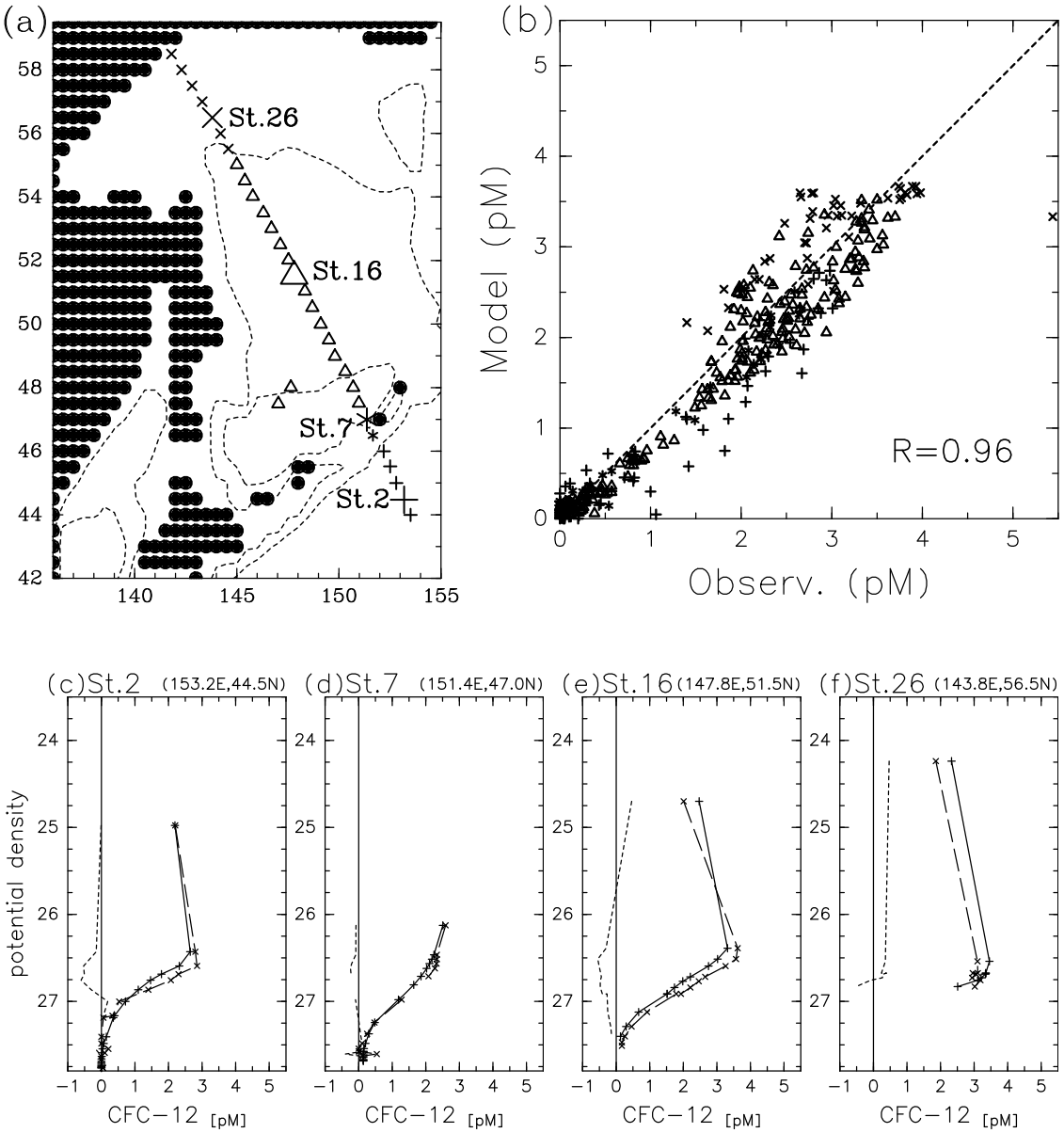

Figure 6. (a) Stations of the NODC Cruise SU-14129 in WOD, with the contors of isobaths, 500 m and 2500 m. (b) Scatterplot between the data of the NODC Cruise SU-14129 and of the standard experiment in the northwestern shelf (crosses), the central and Kuril Basins (triangles), Bussol' Strait (asterisks), and the Pacific (pluses). (c–f) CFC-12 concentrations at Stations 2, 7, 16, and 26 (see Figure 6a) as a function of the potential density. Solid lines with pluses and broken lines with crosses denote the standard experiment and the WOD, respectively. Dashed line denotes the difference between the two data sets.

our discussions to the areas where observations have not been conducted.

3.1. Comparison With Observations

[22] Before comparing the results of the standard experiment with the observational results, we should note the difference in the year between the YK04's data and the experiment. While the data of YK04 are of 1998, 1999, and 2000, the experiment results shown in the present paper are of 1996 because of the limitation of the OCMIP-2 data period. We consider that this difference has no significant influence on the CFC-12 distribution discussed here since the rate of increase in the atmospheric concentration of CFC-12 was very small in the late 1990s [*Walker et al.*, 2000]. The comparison between the WOD data and the standard experiment is made using data of the same year, 1993.

[23] First, we compared the vertical distributions of the CFC-12 between the model results and the observations. Figure 6b shows a scatterplot of the WOD data and the model results at the points denoted in Figure 6a. The agreement between them is good with a correlation coefficient of 0.96. Vertical profiles of CFC-12 are also well simulated in the model as shown in Figures 6c–6f in which vertical profiles of the CFC-12 concentration are shown as a function of the potential density (σ_θ) at Stations 2, 7, 16, and 26 denoted in Figure 6a, as an example of four regions:

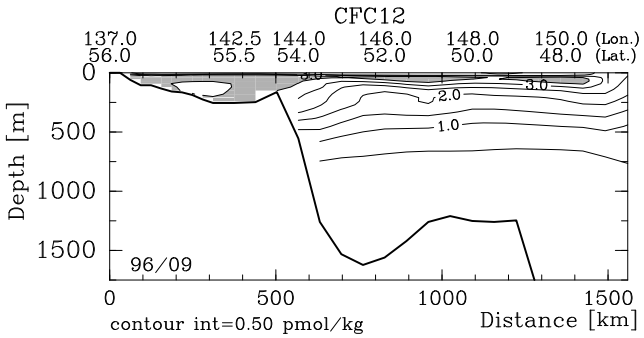

Figure 7. Vertical section of CFC-12 concentration along the line denoted by the solid line in Figure 1a. Areas with CFC-12 concentrations more than 3.5 pmol/kg are shaded.

the Pacific, Bussol' Strait, the central part of the Okhotsk Sea and the northwestern shelf. Based on the data in Figure 6b, we find that the model tends to underestimate the CFC-12 concentration in the Pacific (pluses in Figure 6b; see also Figure 6c) and to overestimate it in the northwestern shelf (crosses in Figure 6b; see also Figure 6f). The underestimate in the Pacific is probably due to the influence from the eastern boundary where CFCs are restored to 0. The overestimate in the northwestern shelf is possibly caused by using the OCMIP-2 ice concentration data in the calculation of the CFC flux at the sea surface, because the concentrations decrease when we use the simulated ice concentration data (see section 5).

[24] The model successfully simulates the CFC-12 concentration along the line observed by YK04 (Figure 7). The maximum concentration larger than 3 pmol/kg is found in the subsurface layer except for the shallow shelf. This subsurface layer corresponds to the dichothermal layer, which is the temperature minimum layer in the subsurface and is a remnant of the winter mixed layer. Below the dichothermal layer, the concentration decreases with depth to about 0.5 pmol/kg at a depth of 750 m. The concentration in this section is highest on the shelf. These features are similar to observations by YK04 (see their Figure 3). The model also captures well the observational features along the 56°N line on the northwestern shelf (open squares in Figure 1): the maximum concentration of about 3.75 pmol/kg in the west and a relatively low concentration wedge of about 3 pmol/kg in the east in both the model results and the observation by YK04 (Figure 8).

[25] Next, horizontal distributions of CFC-12 on the 26.8 σ_θ and 27.4 σ_θ density surfaces are compared (Figure 9). Observed features by YK04 (Figure 10) are well represented in the model results. On the 26.8 σ_θ surface, the highest CFC-12 concentration is found on the northern and the northwestern shelves. Relatively high CFC-12 extends from these shelf areas southward, being squeezed along Sakhalin Island, and spreads over the Kuril Basin. The concentration of CFC-12 decreases from the northwestern shelf toward the Kuril Basin. On the 27.4 σ_θ surface, high CFC-12 is localized around the Kuril Islands with the highest concentration near Bussol' Strait. Overall, the distribution of CFC-12 in the area observed in previous studies are satisfactorily represented in our model simulation. Hence we expect that our model gives a reasonable representation of the CFC-12 distribution in the entire Sea of Okhotsk.

3.2. CFC-12 in the Sea of Okhotsk

[26] The simulated concentration of CFC-12 is generally higher in the Sea of Okhotsk than in the Pacific on the 26.8 σ_θ surface (Figure 9a). This implies that the source of CFC-12 on this density surface is mainly in the Sea of Okhotsk. High concentration of CFC-12 is found on the northern and the northwestern shelves in the Sea of Okhotsk. The distribution of CFC-12 is similar to that of low-temperature water (Figure 4b), suggesting that transport of CFC-12 on this surface is related to the formation of sea ice in winter. Concentration of CFC-12 is highest along the coast where coastal polynyas are found in Figure 3a. This is consistent with the observational studies showing that DSW is formed in coastal polynyas [e.g., *Nihashi et al.*, 2009] and DSW is enriched with CFCs (YK04). In the Kuril Basin, CFC-enriched water from the north mixes with inflowing low CFC water from the Pacific and flows northward in the eastern part of the Sea of Okhotsk. Some portion of CFC-enriched water also flows into the Pacific through Bussol' Strait. In the Pacific, this high CFC signal extends both southward along the Kuril Islands and eastward along the 45°N line. We do not, however, discuss the distribution in the Pacific, where the influence of the open boundaries of the model is considerable. We will study it separately with a more extensive model in the future. On the 27.4 σ_θ surface (Figure 9b), CFC-12 is highest around Bussol' Strait. This illustrates that CFC-12 enters this layer around the strait. The northern part of the Sea of Okhotsk is

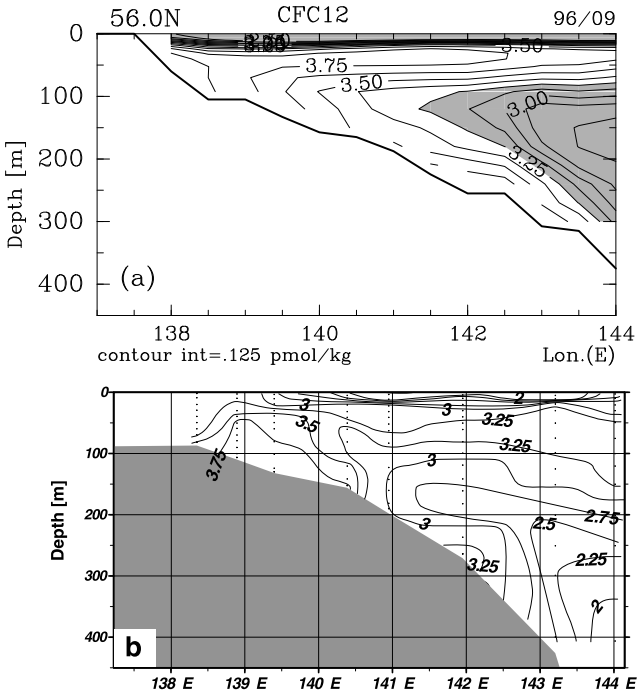

Figure 8. (a) Vertical section of CFC-12 concentration in the standard experiment along the line denoted by open squares in Figure 1a. Areas with CFC-12 concentration less than 3.25 pmol/kg are shaded. (b) Observational results along the near section as Figure 8a quoted from YK04.

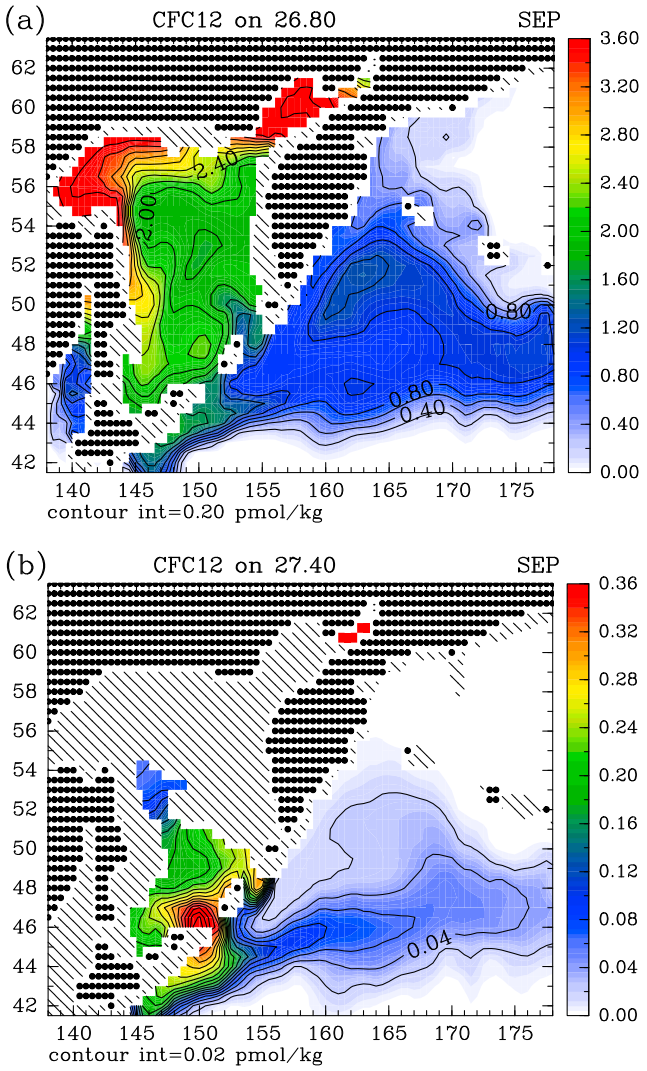

Figure 9. Spatial distributions of CFC-12 concentration in the standard experiment on the (a) 26.8 σ_θ and (b) 27.4 σ_θ density surfaces in September. Hatched regions are occupied with water lighter than each density. The color scales are different in Figures 9a and 9b.

occupied with water lighter than 27.4 σ_θ. These imply that brine rejection exerts little influence on this deep (dense) layer.

[27] Vertical distribution of CFC-12 along the 55.5°N is quite different between the west and the east of the front, i.e., a sharp gradient in the concentration, found around 144°E (Figure 11). On the western side, which is the northwestern shelf and the slope, the CFC-12 concentration is relatively high throughout the water column. On the eastern side, the concentration is low below the depth of the winter mixed layer (about 100 m). On the northwestern shelf, winter cooling and brine rejection transform CFC-enriched surface water into DSW, dense enough to sink to the shelf bottom. This water is, however, not heavy enough to sink below a depth of about 450 m on the slope (143°E–144°E). This is consistent with observations that DSW flows around a depth of a few hundreds meters on the slope [e.g., *Nakatsuka et al.*, 2002; *Mizuta et al.*, 2003; *Fukamachi et al.*, 2004]. In the eastern part of the front, on the other hand, diffusion is the only process to transport CFC-12 directly into the layer below the winter mixed layer. Therefore, the concentration is highest at the dichothermal layer and low in the layer below a depth of 100 m.

[28] YK04 introduced ΔpCFCs to clarify the ventilation processes unique to the Sea of Okhotsk. According to them, we define ΔpCFC as

$$\Delta\mathrm{pCFC}(x, y, \rho, t) = \mathrm{pCFC}(x, y, \rho, t) - \mathrm{pCFC}_{\mathrm{ref}}(\rho, t),$$

where pCFC is the partial pressure of CFC in dry air equilibrated with seawater containing CFC, x, y is the location, ρ is potential density of seawater, t is time, and $\mathrm{pCFC}_{\mathrm{ref}}$ is pCFC at a reference point. The atmospheric concentration of CFC-12 is monotonically increasing during the present simulation period. Therefore, high pCFC-12 indicates that the water was recently in contact with the atmosphere. Thus ΔpCFC-12 is regarded as an index of the ventilation relative to the reference point. When we chose the reference point in the Pacific, ΔpCFC-12 can be a tracer of water ventilated by unique processes to the Sea of Okhotsk. Although in the calculation by YK04 the reference point is set near Bussol' Strait on the Pacific side, this location may not be ideal. Because water flows out from the Sea of Okhotsk to the Pacific through Bussol' Strait (Figure 4a), points near the strait may be influenced by outflowing water from the Sea of Okhotsk. We thus chose a point near Kruzenshterna Strait as the reference point, denoted with a solid star in Figure 12, since Kruzenshterna Strait is an entrance point for waters into the Sea of Okhotsk (Figure 4a). It is noted that the simulated ΔpCFC values need not be comparable with those of YK04's because the reference points are different and the simulated pCFC at the reference point should be too low because of the eastern boundary conditions.

[29] Figure 13a shows the vertical section of ΔpCFC-12 along the line denoted in Figure 12. This line is roughly along a path of water with high CFC-12 concentration; it starts from the northwestern shelf where DSW forms, enters the Kuril Basin, reaches the Kuril Islands, and returns to the northwestern shelf in the cyclonic gyre.

[30] Three distinct features are present in Figure 13a: (1) ΔpCFC-12 is high (> about 100 pptv) in the intermediate layer (from a depth of a few hundred meters to a depth of about 600 m) throughout this vertical section, (2) a wedge of high ΔpCFC-12 (> about 200 pptv) extends in the intermediate layer from the northwestern shelf to the Kuril Islands (from the point No. 1 to No. 36, and from No. 56 to No. 71), and (3) the value is small in the deeper layers but it is not negligible (higher than 25 pptv even at a depth of 1400 m, and ~25 pptv below 1400 m to the bottom (not shown)).

[31] Items 1 and 2 indicate that the intermediate layer is ventilated well (item 1), particularly along the path of DSW (item 2). Item 3 indicates that the deep layers are also weakly ventilated. As *Wong et al.* [1998] and YK04 have discussed, the highest CFC concentration in the dichothermal layer (Figure 7) is due to the open water convection in winter, so that the difference in pCFC of the dichothermal layer between the Sea of Okhotsk and the Pacific is infinitesimal. The difference near the surface is smaller than that in the deeper layer.

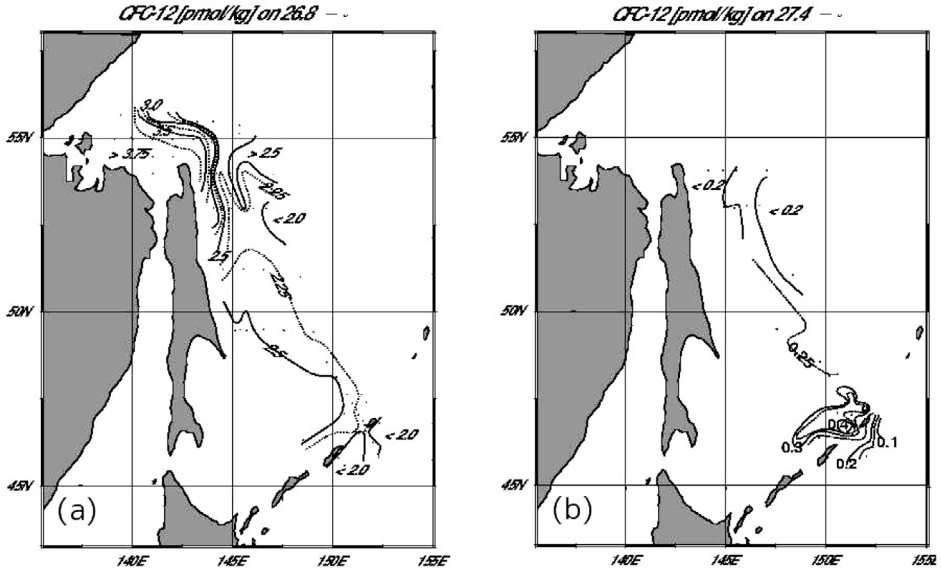

Figure 10. Spatial distributions of CFC-12 observed by YK04 on (a) 26.8 σ_θ and (b) 27.4 σ_θ density surfaces, quoted from YK04.

[32] Figure 14a shows the distribution of ΔpCFC-12 on the 26.9 σ_θ surface, which is the core density of the wedge (Figure 13a). The value of ΔpCFC-12 is highest on the northwestern shelf, and it is relatively high along Sakhalin Island decreasing southward. Figures 13a and 14a indicate that a ventilation source of this intermediate layer is DSW formed on the northern and northwestern shelves.

[33] In the calculation by YK04 (Figure 8 in their paper), the wedge of the high ΔpCFC-12 does not extend to the Kuril Basin, but another maximum of ΔpCFC-12 is found there. Regarding the relatively low ΔpCFC-12 between the wedge and the maximum, YK04 suggested two possible explanations; one is that the section does not follow the flow of DSW, and the other is the presence of eddies in the Kuril Basin [e.g., *Wakatsuchi and Martin*, 1991; *Uchimoto et al.*, 2007]. Figure 14a suggests that the former explanation is more likely to be correct. In fact, when we calculate ΔpCFC-12 along the line denoted in Figure 1 (or Figure 14a), a similar distribution to that of YK04 is obtained (not shown).

[34] The values of ΔpCFC-12 are relatively high in the region around the Kuril Islands. Tidal mixing should also contribute to the high ΔpCFC there. It is, however, difficult to distinguish the influence of tidal mixing from the advection of DSW in the results of the standard experiment alone. This shall be clarified in section 4.

[35] The CFC cumulative flux at the sea surface is the time-integrated flux of the CFC into the sea during the simulation period of about 66 years. The most prominent uptake of CFC-12 occurs around the Kuril Islands, and another prominent uptake occurs near the northern coast (Figure 15a). These uptakes seem to be due to tidal mixing and brine rejection, respectively. Even in experiments with smaller vertical diffusivities along the Kuril Islands (Appendix A), CFC cumulative flux is larger around the Kuril Islands than the northern shelves. Although the flux is also large in the Sea of Japan, the influence of the open boundary is likely to be considerable and thus we do not discuss the Sea of Japan here. In section 4, we discuss the results from experiments without tidal mixing or brine rejection, to separately investigate the effect of each process on the distributions of CFCs.

4. Effects of Tidal Mixing and Brine Rejection

[36] In this section, we discuss two important processes for transporting CFCs into the intermediate and deep layers: tidal mixing around the Kuril Islands and brine rejection. To investigate the role of each process, we conducted two additional experiments; one was an experiment without the tidal mixing parameterization along the Kuril Islands, and the other was an experiment in which brine rejection is suppressed. We refer to these experiments as the NOtide and the NObrine experiments, respectively. In the NObrine

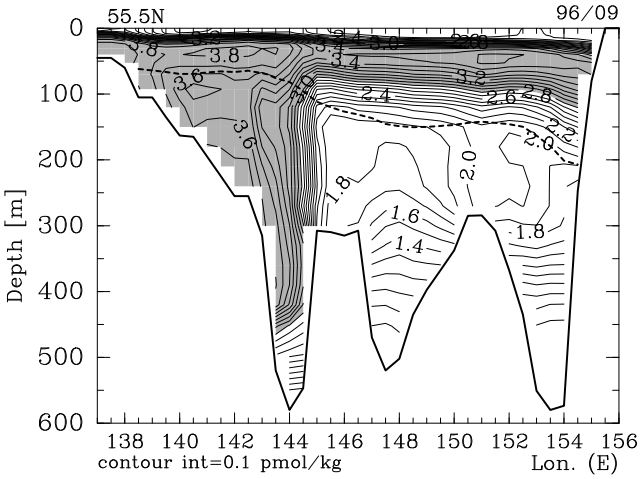

Figure 11. Vertical section of the CFC-12 concentration at 55.5°N in the standard experiment. Areas with values more than 2.8 pmol/kg are shaded. The dashed line indicates the 26.8 σ_θ density surface.

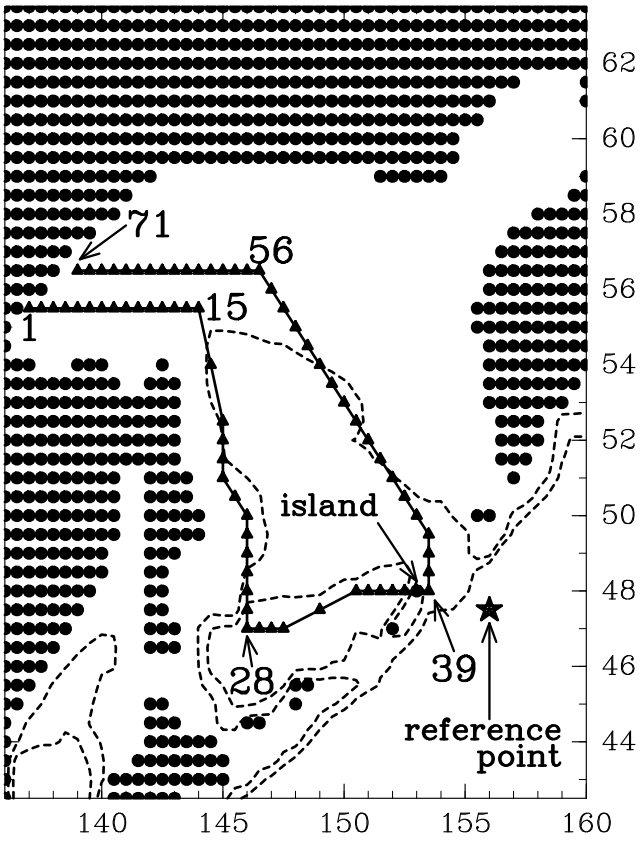

Figure 12. Location of the vertical section shown in Figure 13. Solid triangles along the line denote the grids used for the plotting. Numbers along the line correspond to those on top of Figures 13a–13c. The solid star in the Pacific (156°E, 47.5°N) denotes the reference point used in the calculation of ΔpCFC.

experiment, we set salinity of sea ice to be 30, so that injection of brine from growing sea ice is about 10% of that in the standard experiment. Note that sea ice itself is produced even in the NObrine experiment. Accordingly, dynamical and thermodynamical effects of sea ice are retained.

[37] Figure 16 shows the differences in the CFC-12 concentrations along the 55.5°N section between the standard experiment and the two experiments. The difference is defined as the concentration in the standard experiment minus that in each experiment. Positive (negative) values in Figure 16 indicate that water is ventilated less (more) in the NOtide or NObrine experiments compared to the standard experiment.

[38] The difference between the standard and the NOtide experiments (Figure 16a) is small on the northwestern shelf (in the west of ~ 143°N). This indicates that the CFC-12 sinks to the bottom on this shelf irrespective of the tidal mixing along the Kuril Islands. The difference is, however, large at depths deeper than about 300 m on the slope (143°E–144°E). This indicates that DSW in the NOtide experiment is less dense than produced in the standard experiment and not heavy enough to sink down to depths deeper than 300 m. The difference in density of DSW is due to the change in the SSS on the shelf; tidal mixing along the Kuril Islands pumps salty water from deep layers up to the surface, and the salty water is then transported to the northern shelves to produce saltier and heavier DSW, as discussed by *Nakamura et al.* [2006a] and *Matsuda et al.* [2009].

[39] Difference in CFC-12 concentration between the standard and the NObrine experiments is negative in the

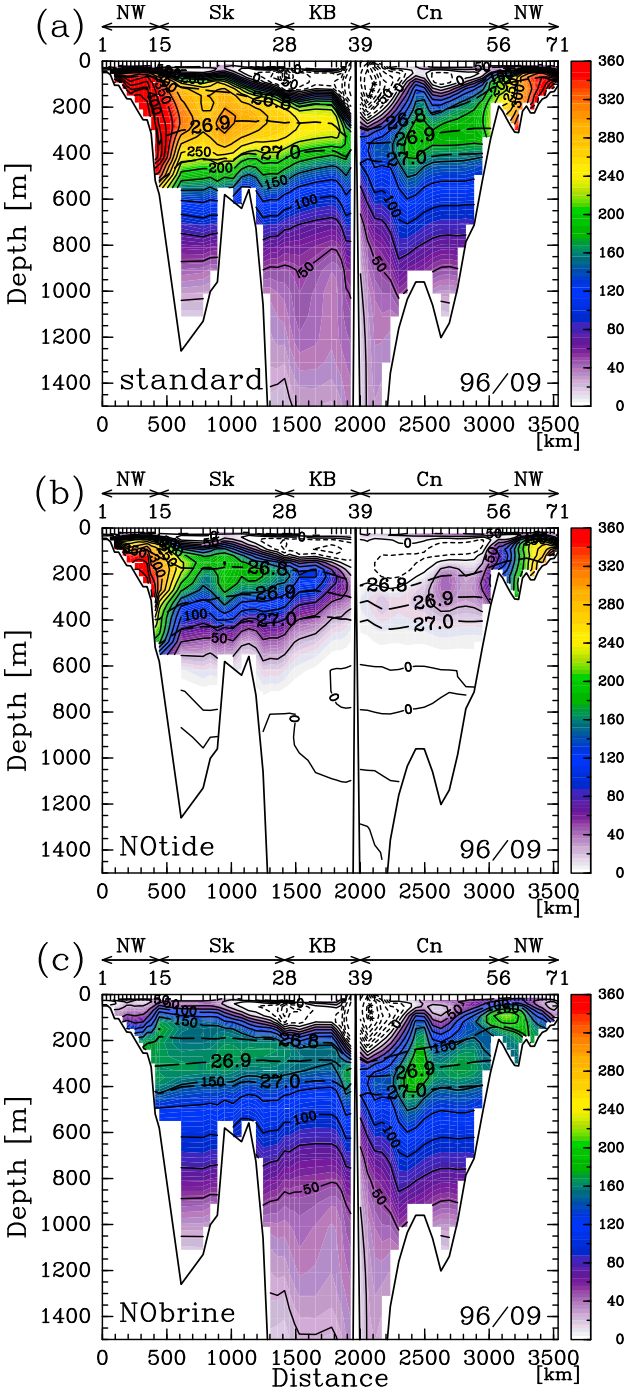

Figure 13. Vertical section of ΔpCFC along the line denoted in Figure 12. (a) The standard, (b) the NOtide, and (c) the NObrine experiments. Broken lines indicate the 26.8 σ_θ, 26.9 σ_θ, and 27.0 σ_θ density surfaces, respectively. Numbers on top of Figures 13a–13c correspond to those in Figure 12. NW, Sk, KB, and Cn indicate regions of the northwestern shelf, along Sakhalin Island, the Kuril Basin, and the center of the Sea of Okhotsk, respectively.

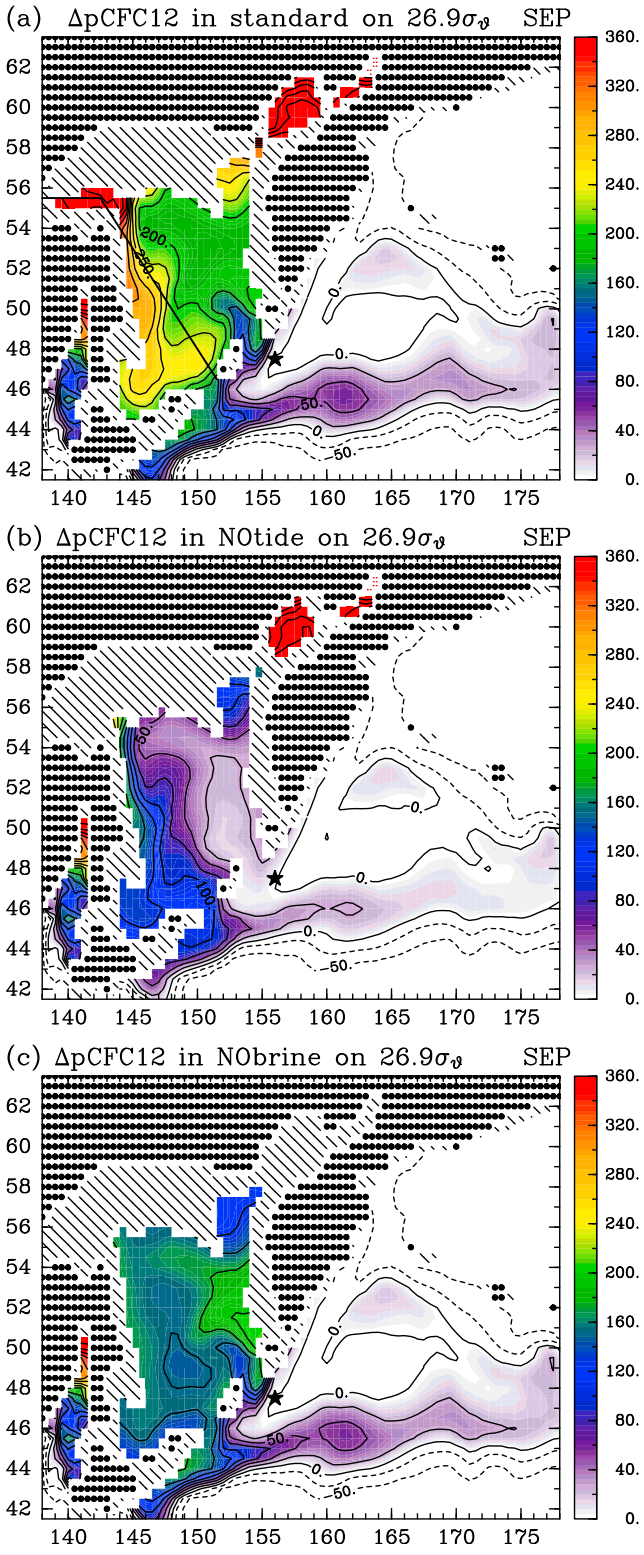

Figure 14. Spatial distribution of ΔpCFC on the 26.9 σ_θ surface in September in (a) the standard, (b) the NOtide, and (c) the NObrine experiments. Hatched regions are occupied with water lighter than 26.9 σ_θ. The line in Figure 14a is the same line as in Figure 1a, and the solid star denotes the reference point.

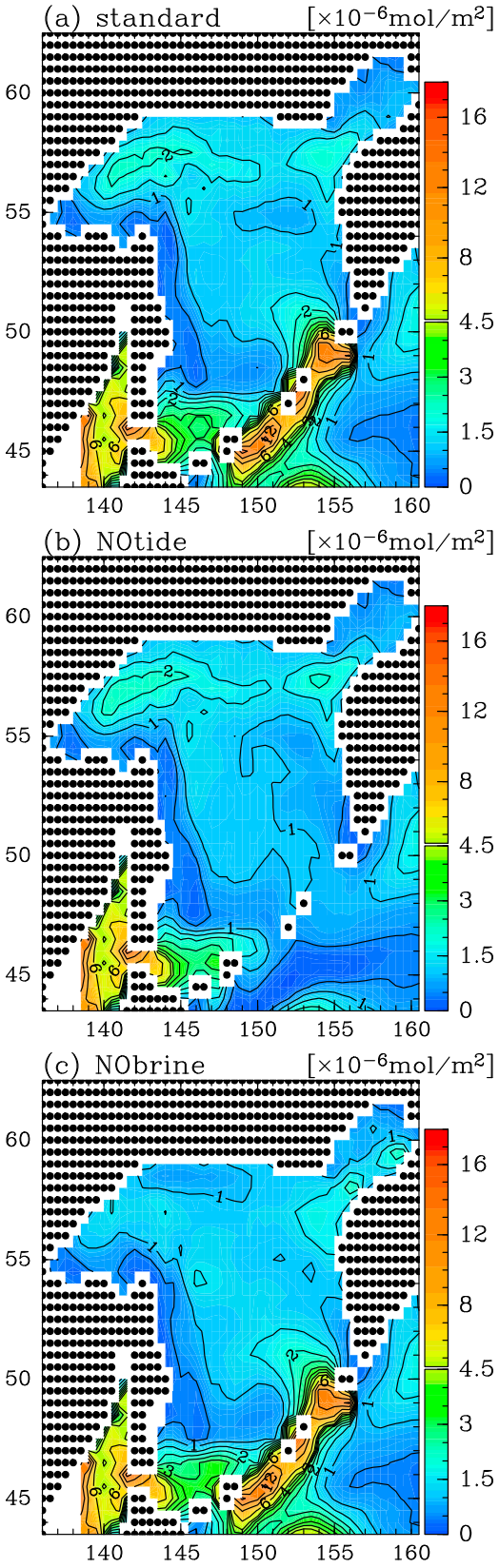

Figure 15. Cumulative CFC-12 flux at the sea surface in (a) the standard, (b) the NOtide, and (c) the NObrine experiments. Contour intervals are 0.5 × 10^{-6} mol/m^2 in less than 4.5 × 10^{-6} mol/m^2, and 3.0 × 10^{-6} mol/m^2 in larger than 4.5 × 10^{-6} mol/m^2.

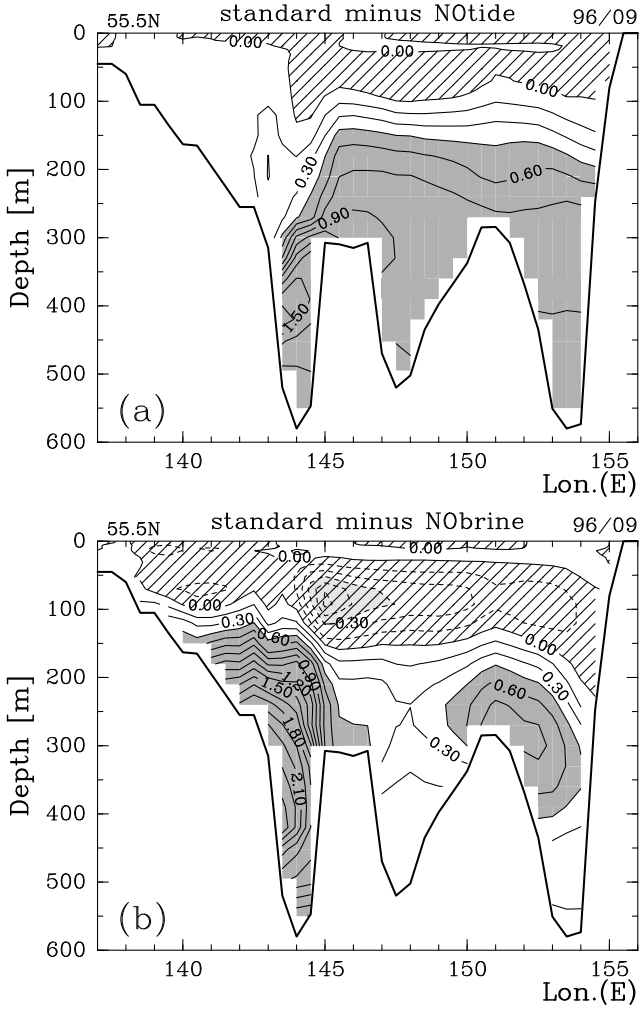

Figure 16. Differences in the CFC-12 concentration between (a) the standard and NOtide experiments, and (b) the standard and NObrine experiments, along the 55.5°N line in September. Positive (negative) values indicate that water is ventilated less (more) in NOtide or NObrine experiments than standard experiment. Negative areas are hatched. Areas with absolute values larger than 0.45 are shaded densely (positive) or lightly (negative).

shallower layer and positive in the deeper layer on the whole of the section (Figure 16b). Without brine rejection, DSW is hardly formed, resulting in less ventilated deeper layers on the shelf and the slope. On the other hand, the winter mixed layer in the NObrine experiment becomes somewhat deeper than in the standard experiment, because brine rejection lowers SSS by transporting salt to deeper layer. This is the reason of the negative difference centered at a depth of about 100 m, around which is the bottom of the winter mixed layer.

[40] Further south at 50°N, a large difference between the standard and the NObrine experiments is localized around a depth of 300 m along the western boundary (Figure 17b). Differences are small at the other depths and regions. The large positive difference found in the eastern part of Figure 16b is not seen here. This suggests that DSW formed on the northern shelf with the direct effects of brine rejection extends to 55.5°N in the eastern part, but does not flow further southward. This is also shown in Figure 9a. High concentration of CFC-12 extends southward convexly to ~54°N at around 151°E on the 26.8 σ_θ surface.

[41] In contrast, the difference between the standard and the NOtide experiments is horizontally nearly homogeneous (Figure 17a). The influence of the tidal mixing around the Kuril Islands extends widely into the intermediate layer in the entire Sea of Okhotsk. At the eastern edge of Figure 17a (155.5°E, 50°N) is an island of the Kuril Islands, and the relatively large difference in the subsurface layer (shallower than 200 m) reflects the direct effects of tidal mixing. Since surface CFC-enriched water continuously mixes with CFC-depleted water in the deep layers there in the standard experiment, the CFC concentration tends to be low.

[42] The difference between the standard and the NOtide experiments extends over larger areas than that between the standard and the NObrine experiments (Figures 16 and 17). This indicates that tidal mixing along the Kuril Islands plays the major role in ventilation of the intermediate and deep layers, and that brine rejection has a secondary role. The influences of brine rejection are found only in limited areas and depths: on the northern and northwestern shelves and

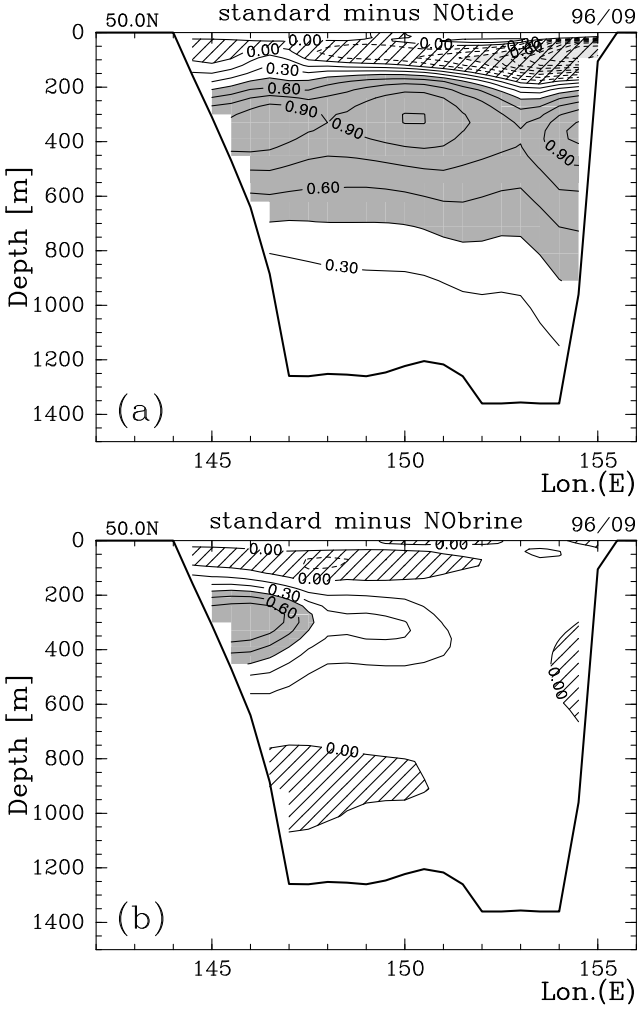

Figure 17. Same as Figure 16, except for along the 50°N line.

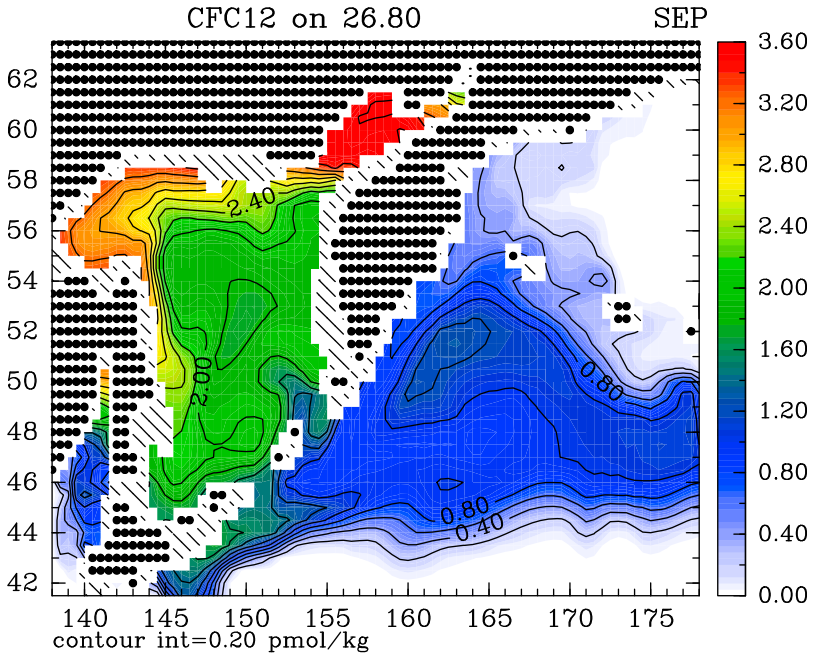

Figure 18. Spatial distribution of CFC-12 concentration on the 26.8 σ_θ density surfaces in September in the Model-ice experiment.

the intermediate layer along Sakhalin Island that corresponds to the path of DSW.

[43] Effects of the two processes on the ventilation are clearly represented in sections of ΔpCFC in the NOtide and NObrine experiments (Figures 13b and 13c). Note that Figures 13b and 13c show the simulated ΔpCFC in the NOtide and NObrine experiments, not differences from the standard experiment. They illustrate the effects of brine rejection (NOtide; Figure 13b) and tidal mixing along the Kuril Islands (NObrine; Figure 13c), respectively. Only one of the three features in the standard experiment (items in section 3.2) remains in the NOtide experiment: the wedge of high values in the intermediate layer (item 2). Further, the value is extremely small in all areas except in the wedge. Conversely, the other two features (items 1 and 3) remain and the wedge (item 2) disappears in the NObrine experiment. Even though the wedge disappears, ΔpCFC there is not small in the NObrine experiment. In the horizontal distribution of ΔpCFC-12 on the 26.9 σ_θ surface ΔpCFC is generally small in the NOtide experiment, and decreases from the west to the east (Figure 14b). In the NObrine experiment, on the other hand, ΔpCFC is relatively high throughout the Sea of Okhotsk (Figure 14c).

[44] These results suggest that tidal mixing along the Kuril Islands is responsible for the ventilation of almost the whole region and layers in the Sea of Okhotsk, and that brine rejection is only responsible for the ventilation of the intermediate layer along the path of DSW. We also found that the density and the depth of the maximum ΔpCFC-12 layer in the wedge in the NOtide experiment are lighter and shallower than those in the standard experiment; they are about 26.8 σ_θ and at about 200 m in the former and 26.9 σ_θ and 300 m in the latter, respectively (Figures 13b and 13a). This is because DSW formed on the northwestern shelf in the NOtide experiment is lighter than that in the standard experiment (Figure 16a). In addition, Figure 14 implies that tidal mixing along the Kuril Islands is more effective for ventilation of the intermediate layer in the North Pacific than brine rejection is. We avoid discussing this area because of the influence of the open boundaries as noted in section 3.2.

[45] The cumulative flux of CFC-12 in the two experiments (Figures 15b and 15c) clearly indicates the ventilation sources of the Okhotsk Sea water. The very large flux found around the Kuril Islands in the standard experiment (Figure 15a) is absent in the NOtide experiment (Figure 15b). The other large flux around the northwestern shelf in the standard experiment disappears in the NObrine experiment (Figure 15c). Therefore the large uptake of CFCs in regions around the Kuril Islands and on the shelves in the north is related to tidal mixing and the brine rejection, respectively.

[46] The larger cumulative CFC flux around the Kuril Islands means that the CFC uptake by tidal mixing is larger than that by brine rejection. Vertical CFC transport from the surface to the deep layers decreases surface CFC concentrations and leads to further oceanic CFC uptake into the surface layer from the atmosphere. Tidal mixing vertically transports CFCs throughout the year, though brine rejection transports them only in winter. This durational difference is a reason of the larger CFC uptake by tidal mixing. In addition, tidal mixing keeps SST low even in summer. The low SST increases surface CFC solubility and facilitates oceanic CFC uptake. The combined effect of the all-year CFC transport and larger CFC solubility around the Kuril Islands explains the larger cumulative CFC flux by tidal mixing.

5. Effect of Ice Concentration Data in CFC Flux

[47] In this study, the CFC flux between the atmosphere and the ocean is calculated with the ice concentration data

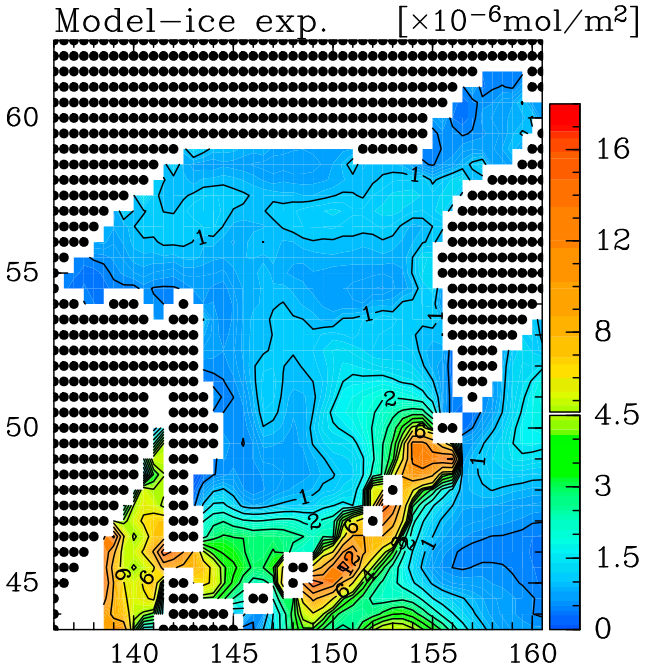

Figure 19. Cumulative CFC-12 flux at the sea surface in the Model-ice experiment. Contour intervals are 0.5×10^{-6} mol/m^2 in less than 4.5×10^{-6} mol/m^2, and 3.0×10^{-6} mol/m^2 in more than 4.5×10^{-6} mol/m^2.

provided by OCMIP-2, not the data calculated in the model. Therefore CFCs enter the model ocean in the ice covered regions where little gas exchange should occur. This may have significantly influenced the concentration of CFCs, so that we performed again the standard experiment calculating the CFC flux with the model's own ice concentration data. The other conditions are the same as in the standard experiment. We refer to this experiment as the Model-ice experiment.

[48] Figure 18 shows the concentration of CFC-12 on the 26.8 σ_θ surface in the Model-ice experiment. We found that the CFC-12 concentrations in the standard experiment (Figure 9a) are estimated higher than in the Model-ice experiment. The increase on the 26.8 σ_θ surface is largest over the northwestern shelf, where it varies between 15% and 25%, depending on the month. Elsewhere, increases < 15% are found along the coast of Sakhalin Island. We also calculated the increase at the sea surface. It is large in the ice covered season but it is not more than 25% in the northwestern shelf and not more than 15% in the other areas.

[49] The CFC cumulative flux at the sea surface in the Model-ice experiment is shown in Figure 19. The flux decreases especially in the northwestern shelf. Still, the local maximum of the flux, although it is weak, is seen in the northwestern shelf.

[50] More CFC-12 enters the sea through gas exchange in the ice covered regions in the standard experiment than in the Model-ice experiment. However, the ice concentration in the model is somewhat higher as described in section 2.3 (Figure 3). This suggests that using the model's own ice concentration data does not necessarily lead to a better simulation than using the OCMIP-2 ice data, and that it may underestimate the CFC-12 concentration. Therefore, we may regard the discussions in the former sections as reasonable, although the effects of brine rejection may be somewhat overestimated.

6. Summary and Concluding Remarks

[51] We successfully simulated the distribution of CFCs in the Sea of Okhotsk. Our simulation clearly illustrates that ventilation sources of the intermediate layer are two areas, on the northwestern and northern shelves and around the Kuril Islands. The area around the Kuril Islands is also the ventilation source of the deep layers. The mechanisms of the ventilation in these two areas are convection due to brine rejection and tidal mixing, respectively.

[52] We conducted two additional experiments, in which one of the two mechanisms is excluded. Through these experiments, we evaluated the effects of each mechanism separately and revealed the following.

[53] 1. Brine rejection on the northwestern and northern shelves leads to the ventilation of the intermediate layer but its effect is limited to areas near the northern coast and in the western part of the sea along the flow of DSW from the northwestern shelf to the Kuril Basin along Sakhalin Island.

[54] 2. Tidal mixing around the Kuril Islands ventilates the intermediate layer throughout the Sea of Okhotsk. The intermediate layer along the east coast of Sakhalin Island is ventilated without brine rejection, although the strength is weaker. Tidal mixing also affects the depth and density of DSW formed on the northwestern shelf owing to preconditioning [*Nakamura et al.*, 2006a], and thus those of the layer of the maximum ΔpCFC.

[55] 3. The tidal mixing also ventilates deeper layers of the entire basin.

[56] The present study shows that tidal mixing and brine rejection are indispensable for the ventilation of layers deeper than the winter mixed layer in the Sea of Okhotsk. Because density surfaces denser than 26.8 σ_θ do not outcrop in the North Pacific, the Sea of Okhotsk is the ventilation area for intermediate layers of the North Pacific. Therefore, these mechanisms in the Sea of Okhotsk should be incorporated in models to better represent water properties in the North Pacific intermediate layer. Although we do not discuss details of the distributions of CFCs in the North Pacific where the model boundaries have significant influences, CFCs from the Sea of Okhotsk spread over the subarctic gyre (e.g., Figure 9). With a model covering a larger area, we will be able to study the distribution of well-ventilated Okhotsk Sea water in the North Pacific. Nevertheless, through simulations of CFCs, the present model proves to be reasonably good to represent processes in the Sea of Okhotsk.

[57] Observational studies have shown that the outflow from the Sea of Okhotsk plays a role in transportation of biogeochemical materials in the North Pacific [*Nakatsuka et al.*, 2002, 2004a, 2004b; *Chen et al.*, 2004; *Nishioka et al.*, 2007]. The outflow from the Sea of Okhotsk also transports a large amount of anthropogenic CO_2 into the North Pacific [*Ono et al.*, 2003]. The present study implies that the two ventilation mechanisms should be

incorporated to simulate those materials in and around the Sea of Okhotsk.

Appendix A: Simulations With Different Tidal Mixing Parameterizations Along the Kuril Islands

[58] We have carried out four simulations with smaller vertical diffusivities applied along the Kuril Islands than for the standard experiment (cases A, B, C, and D in Figure 2). In two profiles (cases A and B), the values from the bottom to 700 m above the bottom are smaller than for the standard experiment. In the cases C and D, vertical diffusivities are one fifth and two-fifths of that of those for the standard experiment, respectively.

[59] As the diffusivities decrease, the cumulative flux of CFC-12 along the Kuril Islands becomes smaller. However, even in the case of the smallest diffusivities (case D), the cumulative flux is much larger around the Kuril Islands than in the northwestern shelf region (Figure A1). Therefore, our conclusion that tidal mixing along the Kuril Islands incorporates more CFCs into the sea surface layer than brine rejection is not due to the use of too large diffusivity values.

[60] On the other hand, the CFC concentration in the deep layers decreases as the diffusivities decrease. Even in the largest diffusivity case (case A) of the four, the CFC-12 concentration on 27.4 σ_θ surface (Figure A2) is not as high as that in the standard experiment that is equivalent to the observation (Figure 9b). In the other three cases, the maximum concentrations on the 27.4 σ_θ surface are lower (0.32, 0.16 and 0.08 in order from cases B–D, respectively).

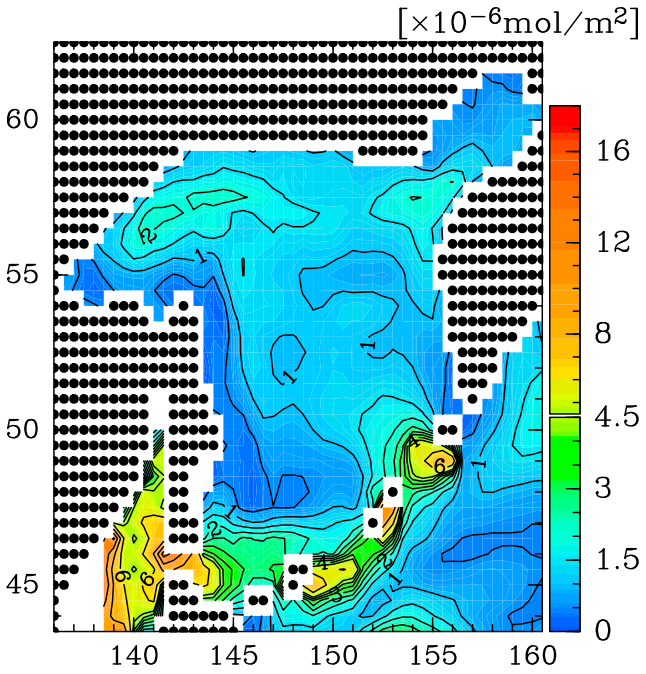

Figure A1. Cumulative CFC-12 flux at the sea surface in case D. Contour intervals are 0.5×10^{-6} mol/m^2 in less than 4.5×10^{-6} mol/m^2, and 3.0×10^{-6} mol/m^2 in more than 4.5×10^{-6} mol/m^2.

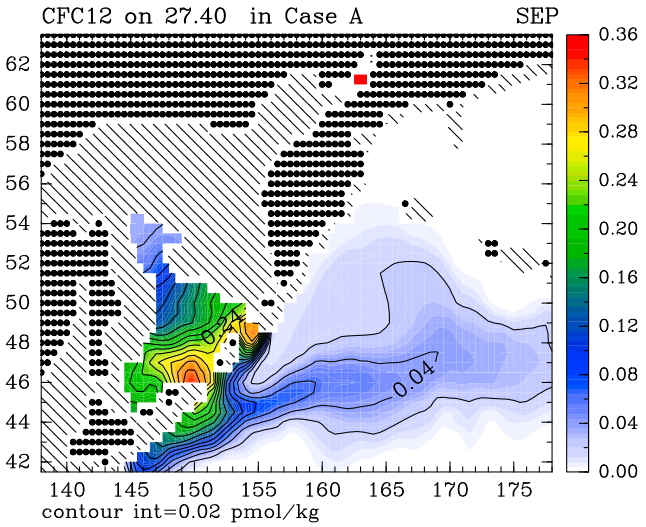

Figure A2. Spatial distributions of CFC-12 concentration on the 27.4 σ_θ density surface in case A.

Therefore, to simulate a CFC distribution similar to the observed one, such large diffusivities as in the standard experiment are necessary at least in coarse resolution models like the present one.

[61] **Acknowledgments.** We thank H. Hasumi and T. Ono for their useful comments. We are indebted to K. Ono for showing us unpublished observational data at Bussol' Strait, which was useful for the parameterization of tidal mixing along the Kuril Islands. This paper was improved greatly thanks to comments from P. Chapman and the two anonymous reviewers. Numerical calculations were performed on the Pan-Okhotsk Information System of Institute of Low Temperature Science, Hokkaido University, and the supercomputer, HITACHI SR11000, at information initiative center, Hokkaido University. This study was supported by the New Energy and Industrial Technology Development Organization (NEDO), and the collaborative research program 2009, information initiative center, Hokkaido University. The figures were produced by GFD-DENNOU Library (http://www.gfd-dennou.org/index.html.en).

References

Adcroft, A., C. Hill, and J. Marshall (1997), Representation of topography by shaved cells in a height coordinate ocean model, *Mon. Weather Rev.*, *125*, 2293–2315.

Chen, C.-T. A., A. Andreev, K.-R. Kim, and M. Yamamoto (2004), Roles of continental shelves and marginal seas in the biogeochemical cycles of the North Pacific Ocean, *J. Oceanogr.*, *60*, 17–44.

Conkright, M. E., R. A. Locarnini, H. E. Garcia, T. D. O'Brien, T. P. Boyer, C. Stephens, and J. I. Antonov (2002), *World Ocean Atlas 2001, CD-ROM documentation*, 17 pp., Natl. Oceanogr. Data Cent., Silver Spring, Md.

Cox, M. D. (1987), Isopycnal diffusion in a z-coordinate ocean model, *Ocean Modell.*, *74*, 1–5.

Dutay, J.-C., et al. (2002), Evaluation of ocean model ventilation with CFC-11: Comparison of 13 global ocean models, *Ocean Modell.*, *4*, 89–120.

Fine, R. A., K. A. Maillet, K. F. Sullivan, and D. Willey (2001), Circulation and ventilation flux of the Pacific Ocean, *J. Geophys. Res.*, *106*, 22,159–22,178.

Fukamachi, Y., G. Mizuta, K. I. Ohshima, L. D. Talley, S. C. Riser, and M. Wakatsuchi (2004), Transport and modification processes of dense shelf water revealed by long-term moorings off Sakhalin in the Sea of Okhotsk, *J. Geophys. Res.*, *109*, C09S10, doi:10.1029/2003JC001906.

Gent, P. R., J. Willebrand, T. J. McDougall, and J. C. McWilliams (1995), Parameterizing eddy induced tracer transports in ocean circulation models, *J. Phys. Oceanogr.*, *25*, 463–474.

Hasumi, H. (2006), CCSR ocean component model (COCO) version 4.0, *CCSR Rep.*, *25*, 103 pp.

Hunke, E. C., and J. K. Dukowicz (1997), An elastic-viscous-plastic model for sea ice dynamics, *J. Phys. Oceanogr.*, *27*, 1849–1867.

Ishida, A., Y. Sasai, and Y. Yamanaka (2007), Role of eddies in chlorofluorocarbon transport in wind-driven oceanic layers, *J. Phys. Oceanogr.*, *37*, 2491–2508.

Itoh, M., K. I. Ohshima, and M. Wakatsuchi (2003), Distribution and formation of Okhotsk Sea Intermediate Water: an analysis of isopycnal climatological data, *J. Geophys. Res.*, *108*(C8), 3258, doi:10.1029/2002JC001590.

Itoh, S. (2008), Observations of current and turbulence within the Urup Strait (in Japanese), *Kaiyo Monthly Ex.*, *50*, 77–84.

Johnson, D. R., T. P. Boyer, H. E. Garcia, R. A. Locarnini, O. K. Baranova, and M. M. Zweng (2009), World Ocean Database 2009 documentation, edited by S. Levitus, *NODC Internal Rep. 20*, 175 pp., NOAA Print. Off., Silver Spring, Md.

Kimura, N., and M. Wakatsuchi (2004), Increase and decrease of sea ice area in the Sea of Okhotsk: Ice production in coastal polynyas and dynamic thickening in convergence zones, *J. Geophys. Res.*, *109*, C09S03, doi:10.1029/2003JC001901.

Kitani, K. (1973), An oceanographic study of the Okhotsk Sea: particularly in regard to cold waters, *Bull. Far Seas Fish. Res. Lab.*, *9*, 45–77.

Leonard, B. P., M. K. MacVean, and A. P. Lock (1994), The flux-integral method for multi-dimensional convection and diffusion, *NASA Tech. Memo.*, *106679*, 29 pp.

Martin, S., R. Drucker, and K. Yamashita (1998), The production of ice and dense shelf water in the Okhotsk Sea polynyas, *J. Geophys. Res.*, *103*(C12), 27,771–27,782.

Matsuda, J., H. Mitsudera, T. Nakamura, K. Uchimoto, T. Nakanowatari, and N. Ebuchi (2009), Wind and buoyancy driven intermediate-layer overturning in the Sea of Okhotsk, *Deep Sea Res., Part I*, *56*, 1401–1418.

Mecking, S., and M. J. Warner (2001), On the subsurface CFC maxima in the subtropical North Pacific thermocline and their relation to mode-waters and oxygen maxima, *J. Geophys. Res.*, *106*(C10), 22,179–22,198.

Mizuta, G., Y. Fukamachi, K. I. Ohshima, and M. Wakatsuchi (2003), Structure and seasonal variability of the East Sakhalin Current, *J. Phys. Oceanogr.*, *33*, 2430–2445.

Nakamura, T., and T. Awaji (2004), Tidally induced diapycnal mixing in the Kuril Straits and its role in water transformation and transport: A three-dimensional nonhydrostatic model experiment, *J. Geophys. Res.*, *109*, C09S07, doi:10.1029/2003JC001850.

Nakamura, T., T. Awaji, T. Hatayama, K. Akitomo, T. Takizawa, T. Kono, Y. Kawasaki, and M. Fukasawa (2000), The generation of large-amplitude unsteady Lee waves by subinertial K_1 tidal flow: A possible vertical mixing mechanism in the Kuril Straits, *J. Phys. Oceanogr.*, *30*, 1601–1621.

Nakamura, T., T. Toyoda, Y. Ishikawa, and T. Awaji (2006a), Enhanced ventilation in the Okhotsk Sea through tidal mixing at the Kuril Straits, *Deep Sea Res.*, *53*, 425–448.

Nakamura, T., T. Toyoda, Y. Ishikawa, and T. Awaji (2006b), Effects of tidal mixing at the Kuril Straits on North Pacific ventilation: Adjustment of the intermediate layer revealed from numerical experiments, *J. Geophys. Res.*, *111*, C04003, doi:10.1029/2005JC003142.

Nakamura, T., Y. Isoda, H. Mitsudera, S. Takagi, and M. Nagasawa (2010), Breaking of unsteady lee waves generated by diurnal tides. *Geophys. Res. Lett.*, *37*, L04602, doi:10.1029/2009GL041456.

Nakanowatari, T., K. I. Ohshima, and M. Wakatsuchi (2007), Warming and oxygen decrease of intermediate water in the northwestern North Pacific, originating from the Sea of Okhotsk, 1955–2004, *Geophys. Res. Lett.*, *34*, L04602, doi:10.1029/2006GL028243.

Nakatsuka, T., C. Yoshikawa, M. Toda, K. Kawamura, and M. Wakatsuchi (2002), An extremely turbid intermediate water in the Sea of Okhotsk: Implication for the transport of particulate organic matter in a seasonally ice-bound sea, *Geophys. Res. Lett.*, *29*(16), 1757, doi:10.1029/2001GL014029.

Nakatsuka, T., T. Fujimune, C. Yoshikawa, S. Noriki, K. Kawamura, Y. Fukamachi, G. Mizuta, and M. Wakatsuchi (2004a), Biogenic and lithogenic particle fluxes in the western region of the Sea of Okhotsk: Implications for lateral material transport and biological productivity, *J. Geophys. Res.*, *109*, C09S13, doi:10.1029/2003JC001908.

Nakatsuka, T., M. Toda, K. Kawamura, and M. Wakatsuchi (2004b), Dissolved and particulate organic carbon in the Sea of Okhotsk: Transport from continental shelf to ocean interior, *J. Geophys. Res.*, *109*, C09S14, doi:10.1029/2003JC001909.

Nihashi, S., K. I. Ohshima, T. Tamura, Y. Fukamachi, and S. Saitoh (2009), Thickness and production of sea ice in the Okhotsk Sea coastal polynyas from AMSR-E, *J. Geophys. Res.*, *114*, C10025, doi:10.1029/2008JC005222.

Nishioka, J., et al. (2007), Iron supply to the western subarctic Pacific: Importance of iron export from the Sea of Okhotsk, *J. Geophys. Res.*, *112*, C10012, doi:10.1029/2006JC004055.

Noh, Y., and H. J. Kim (1999), Simulations of temperature and turbulence structure of the oceanic boundary layer with the improved near-surface process, *J. Geophys. Res.*, *104*(C7), 15,621–15,634.

Ogi, M., Y. Tachibana, F. Nishio, and M. A. Danchenkov (2001), Does the fresh water supply from the Amur River flowing into the Sea of Okhotsk affect sea ice formation?, *J. Meteorol. Soc. Jpn.*, *79*, 123–129.

Ohshima, K. I., T. Watanabe, and S. Nihashi (2003), Surface heat budget of the Sea of Okhotsk during 1987–2001 and the role of sea ice on it, *J. Meteorol. Soc. Jpn.*, *81*, 653–677.

Ohshima, K. I., S. C. Riser, and M. Wakatsuchi (2005), Mixed layer evolution in the Sea of Okhotsk observed with profiling floats and its relation to sea ice formation, *Geophys. Res. Lett.*, *32*, L06607, doi:10.1029/2004GL021823.

Ohshima, K. I., S. Nihashi, E. Hashiya, and T. Watanabe (2006), Interannual variability of sea ice area in the Sea of Okhotsk: Importance of surface heat flux in fall, *J. Meteorol. Soc. Jpn.*, *84*, 907–919.

Ono, K., K. I. Ohshima, T. Kono, M. Itoh, K. Katsumata, Y. N. Volkov, and M. Wakatsuchi (2007), Water mass exchange and diapycnal mixing at Bussol' Strait revealed by water mass properties, *J. Oceanogr.*, *63*, 281–291.

Ono, T., K. Sasaki, and I. Yasuda (2003), Re-estimation of annual anthropogenic carbon input from Oyashio into North Pacific Intermediate Water, *J. Oceanogr.*, *59*, 883–891.

Polzin, K. L., J. M. Toole, and R. W. Schmitt (1995), Finescale parameterizations of turbulent dissipation, *J. Phys. Oceanogr.*, *25*, 306–328.

Röske, F. (2001), An atlas of surface fluxes based on the ECMWF re-analysis —A climatological dataset to force global ocean general circulation models, *Rep. 323*, 31 pp., Max-Planck-Inst. für Meteorol., Hamburg, Germany.

Semtner, A. J., Jr. (1976), A model for the thermodynamic growth of sea ice in numerical investigations of climate, *J. Phys. Oceanogr.*, *6*, 379–389.

Shcherbina, A. Y., L. D. Talley, and D. L. Rudnick (2003), Direct observations of North Pacific ventilation: Brine rejection in the Okhotsk Sea, *Science*, *302*, 1952–1955.

Sun, F., V. S. Kim, B. Huang, and D. Wang (2004), Water exchange between the subpolar and subtropical North Pacific in an OGCM, *Sci. China, Ser. D*, *47*, 37–48.

Talley, L. D. (1991), An Okhotsk Sea water anomaly: implications for ventilation in the North Pacific, *Deep Sea Res.*, *38*, 171–190.

Tanaka, Y, T. Hibiya, and Y. Niwa (2007), Estimates of tidal energy dissipation and diapycnal diffusivity in the Kuril Straits using TOPEX/POSEIDON altimeter data, *J. Geophys. Res.*, *112*, C10021, doi:10.1029/2007JC004172.

Tokieda, T., S. Watanabe, and S. Tsunogai (1996), Chlorofluorocarbons in the western North Pacific in 1993 and formation of North Pacific Intermediate Water, *J. Oceanogr.*, *52*, 475–490.

Uchimoto, K., H. Mitsudera, N. Ebuchi, and Y. Miyazawa (2007), Anticyclonic eddy caused by the Soya Warm Current in an Okhotsk OGCM, *J. Oceanogr.*, *63*, 379–391.

Wakatsuchi, M., and S. Martin (1991), Water circulation in the Kuril Basin of the Okhotsk Sea and its relation to eddy formation, *J. Oceanogr. Soc. Jpn.*, *47*, 152–168.

Walker, S. J., R. F. Weiss, and P. K. Salameh (2000), Reconstructed histories of the annual mean atmospheric mole fractions for the halocarbons CFC-11 CFC-12, CFC-113, and carbon tetrachloride, *J. Geophys. Res.*, *105*(C6), 14,285–14,296.

Warner, M. J., J. L. Bullister, D. Wisegarver, R. Gammon, and R. Weiss (1996), Basin-wide distributions of chlorofluorocarbons CFC-11 and CFC-12 in the North Pacific: 1985–1989, *J. Geophys. Res.*, *101*(C9), 20,525–20,542.

Watanabe, Y. W., K. Harada, and K. Ishikawa (1994), Chlorofluorocarbons in the central North Pacific and southward spreading time of North Pacific intermediate water, *J. Geophys. Res.*, *99*(C12), 25,195–25,213.

Watanabe, Y. W., A. Ishida, M. Tamaki, K. Okuda, and M. Fukasawa (1997), Water column inventories of chlorofluorocarbons and production rate of intermediate water in the North Pacific, *Deep Sea Res.*, *44*, 1091–1104.

Wong, C. S., R. J. Matear, H. J. Freeland, F. A. Whitney, and A. S. Bychkov (1998), WOCE line P1W in the Sea of Okhotsk 2. CFCs and the formation rate of intermediate water, *J. Geophys. Res.*, *103*(C8), 15,625–15,642.

Yagi, M., and I. Yasuda (2008), Turbulence observation in Kuril Straits using density inversions (in Japanese), *Kaiyo Monthly Ex.*, *50*, 85–92.

Yamamoto, M., S. Watanabe, S. Tsunogai, and M. Wakatsuchi (2002), Effects of sea ice formation and diapycnal mixing on the Okhotsk Sea intermediate water clarified with oxygen isotopes, *Deep Sea Res.*, *49*, 1165–1174.

Yamamoto-Kawai, M., S. Watanabe, S. Tsunogai, and M. Wakatsuchi (2004), Chlorofluorocarbons in the Sea of Okhotsk: Ventilation of the

intermediate water, *J. Geophys. Res.*, *109*, C09S11, doi:10.1029/2003JC001919.

K. Misumi and D. Tsumune, Environmental Science Research Laboratory, Central Research Institute of Electric Power Industry, 1646 Abiko, Abiko, Chiba 270-1194, Japan.

H. Mitsudera, T. Nakamura, J. Nishioka, and K. Uchimoto, Pan-Okhotsk Research Center, Institute of Low Temperature Science, Hokkaido University, Kita-19, Nishi-8, Kita-ku, Sapporo, Hokkaido 060-0819, Japan. (uchimoto@lowtem.hokudai.ac.jp)

M. Yamamoto-Kawai, Research Center for Advanced Science and Technology, Tokyo University of Marine Science and Technology, 4-5-7 Konan, Minato-ku, Tokyo 108-8477, Japan.